Geophysical & Astrophysical Fluid Dynamics

Publication details, including instructions for authors and subscription information:
http://www.tandfonline.com/loi/ggaf20

Mathematical background of the Riga dynamo experiment

Agris Gailitis [a]

[a] Institute of Physics, University of Latvia, LV-2169 Salaspils, Latvia

Available online: 16 May 2012

To cite this article: Agris Gailitis (2012): Mathematical background of the Riga dynamo experiment, Geophysical & Astrophysical Fluid Dynamics, DOI:10.1080/03091929.2012.680698

To link to this article: http://dx.doi.org/10.1080/03091929.2012.680698

Geophysical and Astrophysical Fluid Dynamics
2012, 1–14, iFirst

Mathematical background of the Riga dynamo experiment

AGRIS GAILITIS*

Institute of Physics, University of Latvia, LV-2169 Salaspils, Latvia

(*Received 14 October 2011; in final form 29 February 2012*)

The Riga dynamo experiment is a laboratory model of the natural process that is responsible for all environmental magnetic-fields which are generated without human interference. This applies to the field of the Earth, the Sun, stars, and even galaxies which are produced by intense motions of large volumes of good electro-conducting fluids. For our experiment, we use molten sodium – the best liquid electro-conductor available in the laboratory. Approximately 2 m^3 of molten sodium are filled into a prolonged cylinder, at the top of which rotates a propeller powered by 200 kW from two motors. The cylinder is divided by thin coaxial inner walls into three parts: in the inner tube the propeller moves the sodium flow helically downward; in the middle one the sodium flows vertically upward; and the outer part contains liquid sodium at rest. When the propeller speed exceeds a critical value (depending on temperature: around 1800 rpm, corresponding to a sodium flow of 0.6 $m^3 s^{-1}$) then a magnetic-field is spontaneously excited. The field pattern slowly rotates around the vertical axis. To enable self-excitation, the sodium flow had been carefully optimized. This article gives an historical overview about the steps in the mathematical description of the Riga dynamo and the optimization of the sodium flow structure. Our analytical model builds on the Ponomarenko configuration, which we modify in four analytical steps. Firstly, the Ponomarenko model was adopted for finite *Rm*. Then, instead of real generation, we find convective amplification. Secondly, when the outer conductor was replaced with a return tube an absolute instability was attained but at high *Rm*. Thirdly, to lower *Rm* a third, immobile conductor was inserted outside and all sizes optimized to achieve global generation at minimum *Rm*. Adopting these sizes, an experiment was designed and made. Fourthly and finally, the velocity profile was replaced by a trial polynomial to identify the direction in which the flow structure should be corrected.

Keywords: MHD Dynamo; Laboratory experiments

1. Short history of the experiment

A Riga-type experiment was proposed by Prof. Max Steenbeck in 1966 when he visited the Institute of Physics in Salaspils. After having completed the mean-field theory of magnetic-field formation in celestial bodies (Steenbeck *et al*. 1966), Steenbeck was excited by the idea to reproduce the process in the laboratory. In the first instance, his intention was to build a small scale demonstration experiment of the α-effect – a cornerstone in his theory. Indeed, such an experiment has been successfully conducted

*Email: gailitis@sal.lv

ISSN 0309-1929 print/ISSN 1029-0419 online
http://dx.doi.org/10.1080/03091929.2012.680698

(Steenbeck *et al.* 1967, 1968). However, the set-up of a full-scale magnetic-field generation experiment was not so fast and easy. No one had a clear idea of which dynamo schema could serve as the basis of such an experiment. Different models were examined by the author in the following years. The first was a large scale ensemble of many parallel helical flows (figure 1(a)) which reproduces the α-effect (Gailitis 1967). The self-excitation condition in a spherical volume was calculated, but the set-up of a corresponding experiment seemed too expensive for our institute. Years later, and quite independent of our early ideas, a very similar concept was known as the Roberts-Busse dynamo (Roberts 1972, Busse 1975) and a similar experiment was built in Karlsruhe (Müller and Stieglitz 2000, Stieglitz and Müller 2001, 2002). The next considered model contained a number of symmetrically located submerged skew-jets (figure 1(b), Gailitis 1969). Some simplified estimates lead to experimentally feasible values of the critical

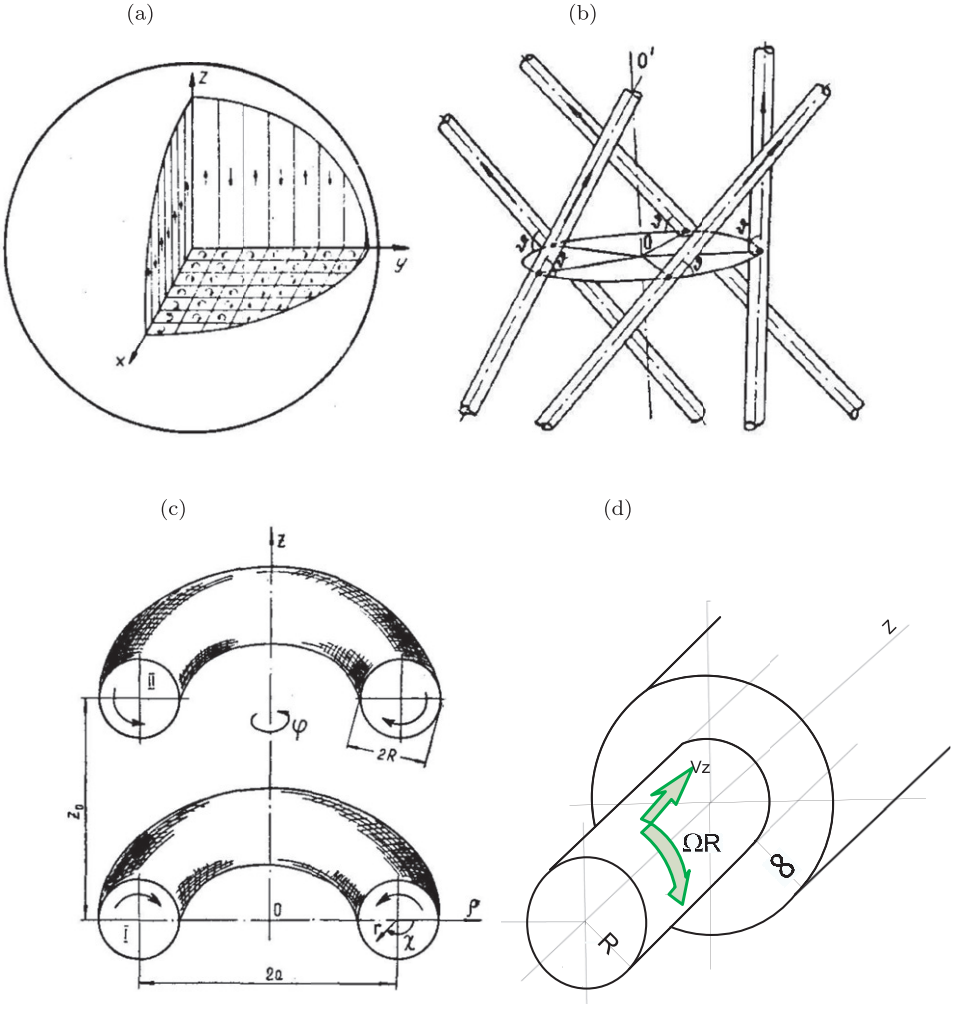

Figure 1. Various theoretical dynamo models: (a) α^2-dynamo setup, (b) Submerged skew-jets, (c) Toroidal vortices and (d) Ponomarenko setup.

magnetic Reynolds number *Rm*. Unfortunately, the more accurate the skin-effect was considered, the higher the critical *Rm* turned out to be. The third model consisted of a pair of toroidal vortices, as shown on figure 1(c) (Gailitis 1970, 1993, 1995). It was mathematically surprising, since the field is produced by a purely meridional flow without any helicity. However, the calculated critical *Rm* proved to be much too large for any realistic experiment. So, we had to abandon that model, too. In total, the search for an appropriate model took 8 years.

In the spring of 1975, on the initiative of Max Steenbek a closed workshop for discussing unintended magnetic-field generation in fast breeder reactors was held at the Obninsk nuclear research center in Russia, where Prof. Subotin drew our attention to a recent article by Ponomarenko (1973). Finally, the concept of the experiment was found on the basis of this article. Shortly, the Ponomarenko concept was further specified (Gailitis and Freibergs 1976, 1980a,b), although its experimental realization took much longer. The first experimental model was set-up in 1986. In 1987, it was tested at the Leningrad Institute for Electrophysical Apparatus where a powerful pump for liquid sodium was available. During this experiment, a significant deformation of the external magnetic-field was observed (Gailitis *et al*. 1987, 1989, Gailitis 1989). Unfortunately, some welding failed due to mechanical vibrations and the experiment had to be stopped before the sodium speed necessary for self-excitation was attained. Rather than repairing this device, in 1994 we started to build a new one at the institute in Salaspils (Gailitis 1996, Stefani *et al*. 1999) shown as a photograph in figure 2 and schematically in figure 3. Since sufficiently strong external pumps were not available, we choose to move the sodium by an internal propeller. To prevent a similar failure as in Leningrad, two full-size water mock-ups were built for various tests of the mechanical integrity and the flow structure. Even the final sodium model was at first tested with water. In 1999, it was filled with sodium, already at the first launch we observed the expected magnetic-field self-excitation (Gailitis *et al*. 2000). For further development, see Gailitis *et al*. (2001a,b,c, 2002, 2004).

2. Ponomarenko approach

Ponomarenko (1973) considered a solid electrical conductor of infinite axial and radial extension with a cylindrical hole shown in figure 1(d). Through this hole, a solid cylinder of the same conductivity is thought to move helically with the axial velocity v_z and angular velocity Ω. The cylinder is in ideal electrical contact with the rigid environment. To find mathematical evidence of magnetic-field generation, Ponomarenko solved the induction equation

$$\left(\frac{\partial}{\partial t} + \boldsymbol{v}\cdot\nabla\right)\boldsymbol{B} = (\boldsymbol{B}\cdot\nabla)\boldsymbol{v} + \frac{1}{Rm}\triangle\boldsymbol{B} \tag{1}$$

both in the rigid conductor and in the mobile cylinder. Because of the symmetry of the problem the magnetic-field eigen-function exponentially depends on the time t, the azimuthal angle φ, and z according to

$$(B_r, B_\varphi, B_z) \sim \exp(\mathrm{i}m\varphi + \mathrm{i}kz + pt).$$

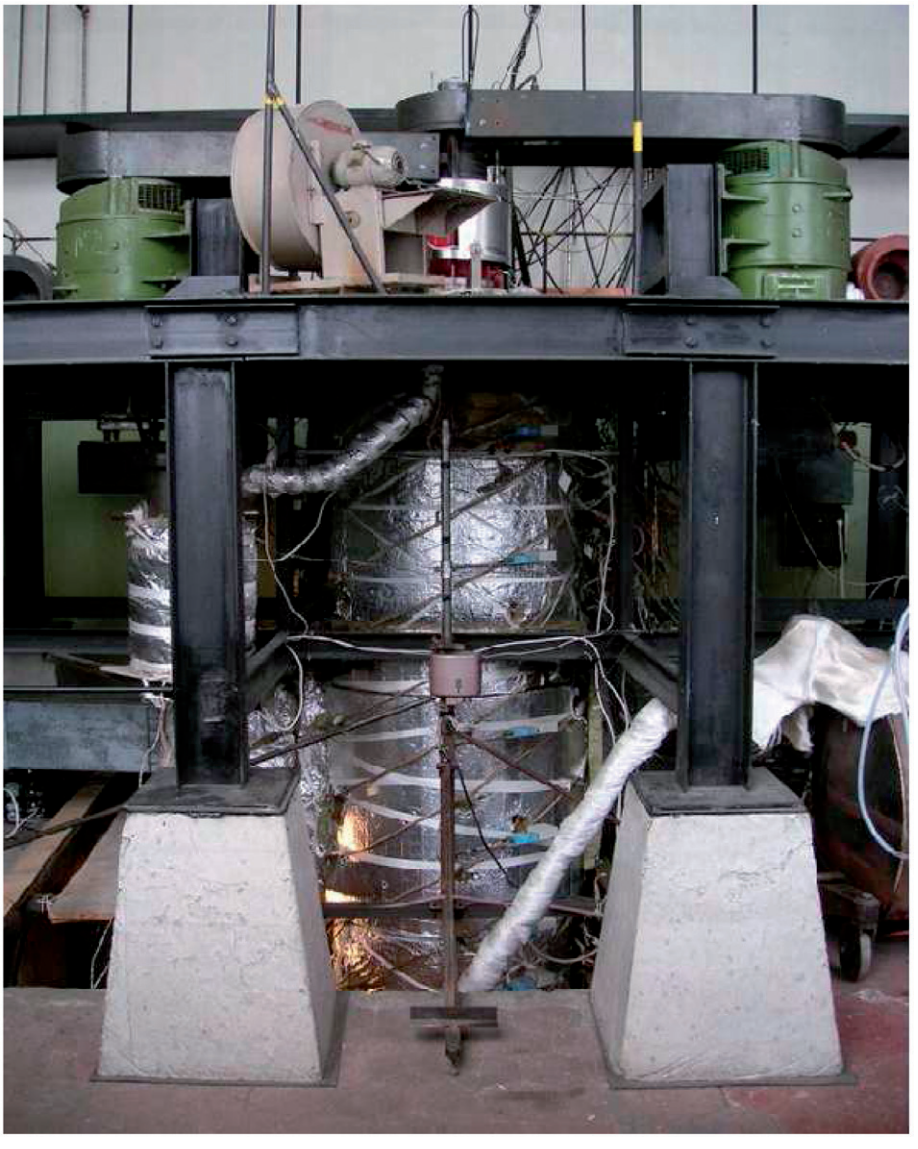

Figure 2. (Colour online). Photograph of the Riga dynamo experiment.

To separate the equations, Ponomarenko considered the complex combination $B_r \pm \mathrm{i}B_\varphi$. Then, the induction equations reduces to Bessel-type equations with complex coefficients having solutions in the form of modified Bessel functions I_m and K_m of complex arguments. In the external domain the equations are

$$\left[\frac{1}{r}\frac{\mathrm{d}}{\mathrm{d}r}\left(r\frac{\mathrm{d}}{\mathrm{d}r}\right) - \frac{(m \pm 1)^2}{r^2} - s^2\right](B_r \pm \mathrm{i}B_\varphi) = 0$$

with

$$s^2 = k^2 + \mu_0 \sigma p.$$

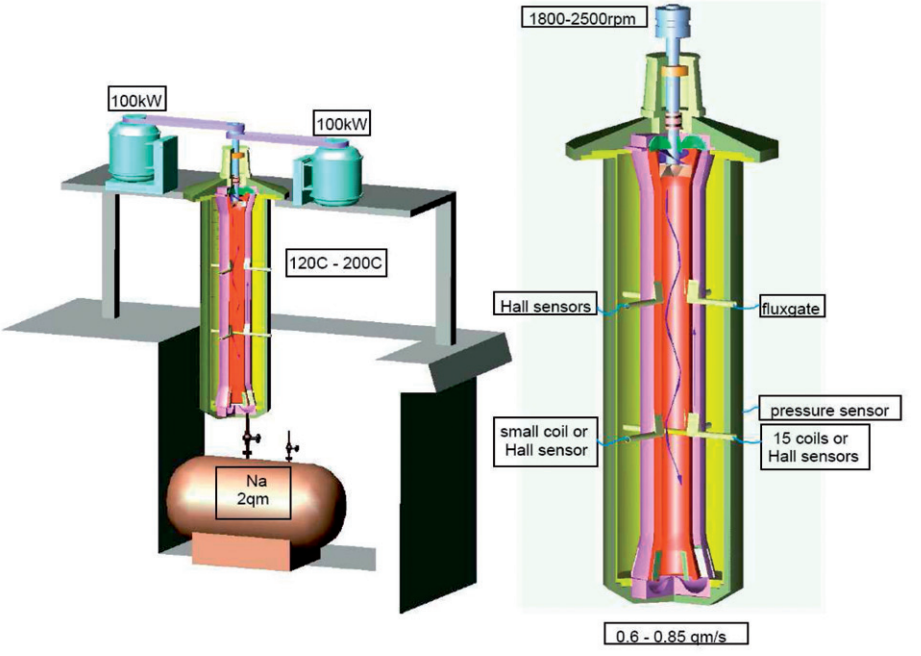

Figure 3. (Colour online). Internal structure of the experiment.

The equations in the moving cylinder differ from those in the immobile conductor only by a Doppler frequency shift $p_{\mathrm{ef}} = p + \mathrm{i}(kv_z + m\Omega)$: instead of s^2, we have

$$q^2 = k^2 + \mu_0\sigma\left[p + \mathrm{i}(kv_z + m\Omega)\right].$$

In the external region, the appropriate solutions, which decay to zero as $r \to \infty$, are

$$B_r \pm \mathrm{i}B_\varphi = b_\pm \mathrm{K}_{m\pm1}(sr),$$

while in the mobile cylinder the solutions regular as $r \to 0$ are

$$B_r \pm \mathrm{i}B_\varphi = a_\pm \mathrm{I}_{m\pm1}(qr).$$

The field continuity condition at the sliding interface ($r = R$) leads to the characteristic equation

$$\Omega\mu_0\sigma R^2(R_+^{-1} - R_-^{-1}) = 2\mathrm{i} \tag{2}$$

with

$$R_\pm = \frac{qR\mathrm{I}_m(qR)}{\mathrm{I}_{m\pm1}(qR)} + \frac{sR\mathrm{K}_m(sR)}{\mathrm{K}_{m\pm1}(sR)}.$$

This is a transcendental equation of the form

$$F(p, k, m, Rm, v_z/\Omega R) = 0. \tag{3}$$

It is complex and contains an integer argument m, two real arguments $Rm = \mu_0\sigma R[v_z^2 + (\Omega R)^2]^{1/2}$, $v_z/\Omega R$ and the two, in general, complex arguments $p = \gamma + \mathrm{i}\omega$ and

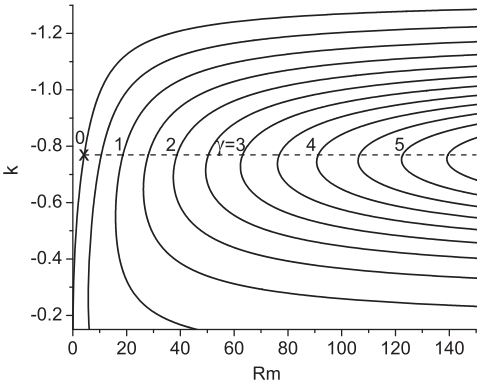

Figure 4. Asymptotic equation (4) numerically solved for (k_r, ω) at $m=1$, $k_i=0$, $v_z=1.3\Omega R$ and selected γ. We present only k_r versus Rm. Ponomarenko prove growing field on dashed line $kv_z=-m\Omega$, $Rm > 4.22m^2$.

$k=k_r+\mathrm{i}k_i$. One can numerically find either one of the complex arguments or any of the two real arguments, say (k_r, ω) in dependence on the other ones.

Actually, Ponomarenko did not solve this equation in a strict sense; he only proved that at large enough Rm there is a solution which is exponentially growing in time (γ positive). For this purpose, Ponomarenko approximated the modified Bessel functions I and K with the three first terms of their asymptotic expansions, which is justified for large arguments sR, qR. Then, the two first terms cancel and the characteristic equation takes the simple form

$$sq(s+q)R = \mathrm{i}m\mu_0\sigma\Omega. \tag{4}$$

The numerically made solution map for this asymptotic characteristic equation is shown in figure 4 for the special ratio $v_z/\Omega R=1.3$ (which turns out to be the optimum value when the exact equation (2) is used). There and below, all lengths measured in units of R and all times in units of $\mu_0\sigma R^2$. We consider only the case $m=1$ as it starts first.

Equation (4) can be converted into an algebraic equation of fourth degree which may be solved even analytically. Ponomarenko followed a simpler route; he just looked at the line $kv_z=-m\Omega$, where $s=q$. The cubic root of both sides of (4) leads to the very simple solution

$$k^2+\mu_0\sigma(\gamma+\mathrm{i}\omega) = (-1)^{1/3}(m\mu_0\sigma\Omega/2R)^{2/3}.$$

At $m\mu_0\sigma\Omega > 2^{5/2}k^3R$ the real part on the right hand side exceeds k^2, hence $\gamma > 0$ and the solution is growing in time. In addition, Ponomarenko proved that with growing value of Rm the maximum of field amplification asymptotically tends to this very line. Figure 4 confirms this behavior. However, it should be noted that resulting condition $Rm > 2^{5/2}\mathrm{m}^2(\Omega R/v_z)^3[1+(v_z/\Omega R)^2]^{1/2}$ is very underestimated. The approximation of Bessel functions by their asymptotic requires much larger Rm.

In summary, Ponomarenko's approach gave a proof in principle of magnetic-field self-excitation, for which the actual numerical value of the threshold was not needed. To find the actual threshold value, we solved the original equation (2) numerically, using

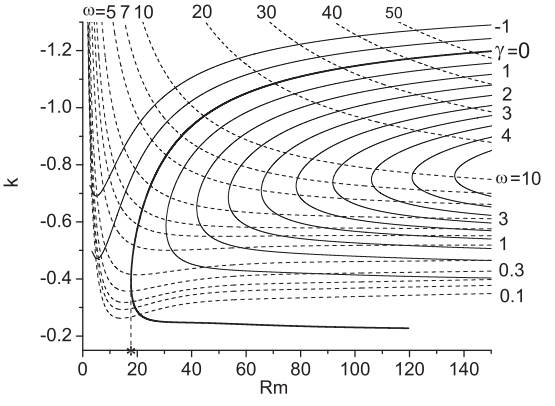

Figure 5. Equation (2) solved numerically for (k_r, ω) at selected γ and for (k_r, γ) at selected ω with $k_i = 0$, $v_z = 1.3\Omega R$.

accurate expressions for Bessel functions (Gailitis and Freibergs 1976). The computed growth curves, including the neutral curve, are shown in figure 5. The fastest growth rate still approaches the line $kv_z = -m\Omega$, but all γ values fall much below the ones given in figure 4. The real generation threshold attains a minimum of $Rm = 17.7$ at $v_z/\Omega R = 1.3$.

3. Problems with the Ponomarenko setup for an experiment

The rather low-value $Rm = 17.7$ seemed attractive for an experiment, but a new problem appeared: p is a complex number whose imaginary part (frequency ω) is shown in figure 5. At the generation threshold the frequency is 0.5 (in units of $1/\mu_0\sigma R^2$). At slightly higher Rm the field grows in some frequency interval round 0.5. As the frequency depends on the wave length, the growing wave packet acquires a positive group velocity. This means that all growing magnetic-field perturbations would move in the direction of the flow with approx. 25% of the axial velocity of the flow. In a real experiment, any growing perturbation would reach the end of the apparatus and the generating process would cease if no new perturbation is created on the other end. In summary, this device would work as an amplifier but not as a generator. Such type of generation is refered to as a *convective instability*. It occurs in many hydrodynamic, plasma physics, vacuum, and solid state electronics phenomena for which a certain direction z is not equivalent to its reflection $-z$. Concepts of convective, absolute, and global instability form a huge subject extending far beyond the scope of this article. Our guidance was derived from a short chapter on pipe flow stability (pages 138–142) in Landau and Lifshitz (1954); for more details, see Pitaevskii and Lifshitz (1981). A famous example of convective instability is the wind tunnel experiment of Schubauer and Skramstad (1947). If a similar experiment were done on the basis of the Ponomarenko model one would observe the magnetic-field amplification in a certain frequency range. The higher Rm, the wider this range, as shown in figure 6. However, the amplification in an experiment of our length seems to be less than three-fold.

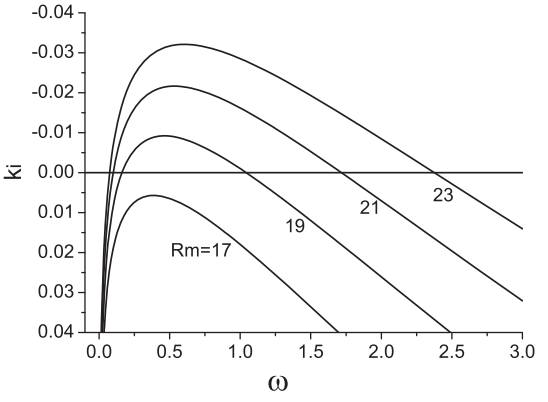

Figure 6. Spatial amplification in a Ponomarenko setup occurring in a certain frequency interval. Equation (2) numerically solved for (k_i, k_r) versus ω at different Rm with $\gamma = 0$ and $v_z = 1.3\Omega R$.

4. Converting Ponomarenko's model into an experiment

To transform the convective instability into a real generation process the equation should have eigen-solutions with zero value at infinity. Otherwise there will be only amplification or deformation of an outside applied field. Due to the properties of the K_m-function, Ponomarenko's solution decays at radial infinity. However, this is not the case for the axial infinity. Therefore, zero boundary conditions should be applied on both ends of the experiment $z = \pm L/2$. These two conditions require the superposition of two $\sim\exp(ikz + i\omega t)$ type solutions, both having the same frequency, but different k values. This cannot be done because, as shown in figure 5, for each frequency there is only one k value. This fact is related to the non-zero group velocity – any single zero has equal frequencies on both sides. Theoretically, the group velocity could be modified by moving the outer conductor in the opposite direction, i.e. by replacing it with a reverse channel. For practical reasons equal flow rates in the direct and in the reverse flow are preferable. Unfortunately, for such a two flow model the critical Rm appears disproportionately large (see the right top corner on figure 10 later in this section). A reasonable compromise is obtained from a model with three volumes of conducting material: the internal cylinder is in helical downward motion; the middle annular region possesses straight upward flow; an outer annular region is filled with sodium at rest (figures 3 and 7); the insulator on the outside is envisaged to be the fourth unbounded volume. If each of these volumes moves as a solid, the solutions are again of the Ponomarenko type. This means, only the I_m-function in the internal cylinder, only K_m-function on the very outside, and a superposition of I_m and K_m in the two annular domains in between. The continuity condition now becomes a complex determinant of the 12th order instead of the simple equation (2). Presentation of the resulting characteristic equation on paper is quite demanding, but it is not a problem to solve it on the computer.

Choosing appropriate channel cross-sections, the group velocity can be significantly reduced or even made equal to zero. The exact zero is not even necessary because the key is to find two solutions with the same frequency but different k and at as small as possible Rm. In the complex plane, the point with zero-group velocity is, by definition, the saddle point for the function $\omega(k)$, and the branch point for the inverse function

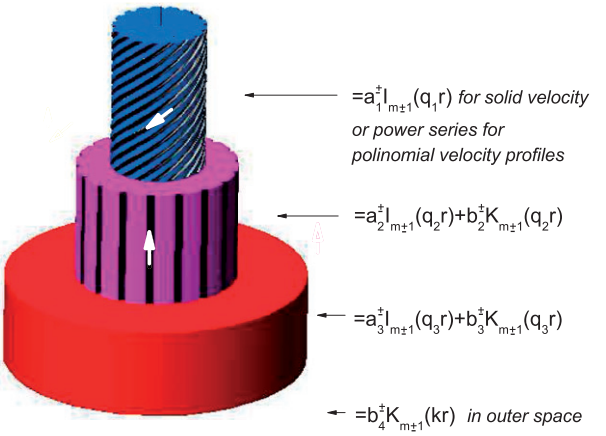

Figure 7. (Colour online). Mathematical model of the Riga dynamo experiment.

$k(\omega)$. The two desired solutions are in the vicinity of this point. Instead of seeking for one-frequency solutions with two different real k (which, in general, does not exist), we need to use wave numbers with some (in practice small) imaginary part k_i. The compatibility condition is still a complex equation of the form (3). The numerical solution for two real arguments (k_r, ω) produces neutral ($\gamma = 0$) curves at different k_i values which are plotted in figure 8(a) with k_r versus Rm and in figure 8(b) with ω versus Rm. The curves in figure 8(a) form an envelope. Its leftmost point corresponds to a zero-complex group velocity. On the whole envelope, the complex group velocity is imaginary. Hence on the upper branch of the $k_i =$ constant curve (before touching the envelope) the real part of group velocity v_{gr} is positive, behind the tangent point it is negative. Figure 8(b) shows that in some k_i range the curves intersect themselves. These intersection points give the desired solution: two different k_r values correspond to the same frequency ω and to the same imaginary part k_i. To see the nodes better, the intersection topology in an expanded form is repeated in figure 8(d). Based on this observation, the computer program can now solve a set of two complex equations of the type of (3):

$$F(p, k, 1, Rm, \text{geometry}) = 0\,, \tag{5a}$$

$$F(p, k + 2\pi/L, 1, Rm, \text{geometry}) = 0 \tag{5b}$$

for four real variables k_r, k_i, ω and Rm. This procedure gives two solutions the superposition which provides a fit for an experiment of length L.

In figure 8(a), three different critical Rm values are marked: Rm^* denotes the convective instability which starts at the leftmost point of the curve $k_i = 0$; Rm^{**} (the leftmost point of the envelope) denotes the absolute instability where magnetic-field generation would start for an infinitely long model; Rm^{***} – the global instability, where generation starts for a finite-length model.

Figure 8(c) gives the shape of the eigenfunction at Rm^* and Rm^{***}. The eigenfunction for Rm^{***} is a superposition of two solutions. This gives a standing wave which differs from the classical standing wave by the amplitude deformed by k_i. The group velocities in both solutions are opposite. The situation is common in optical

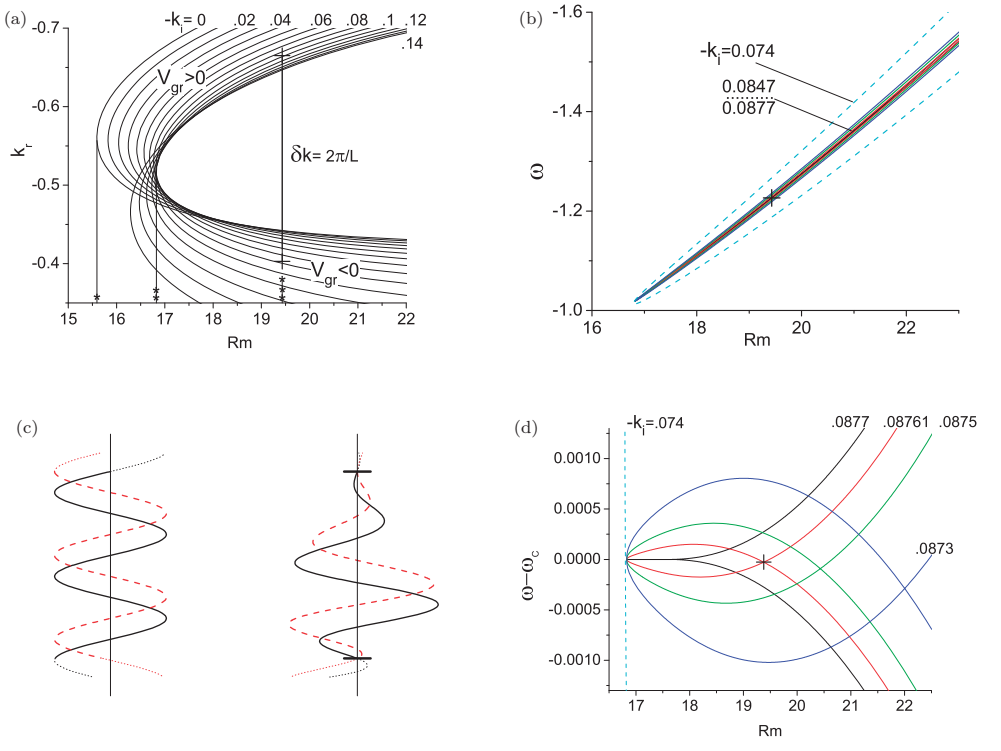

Figure 8. Numerical solution for solid profile model with Riga setup proportions at different k_i. $\gamma = 0$. Expected threshold conditions are marked by crosses +. (a) Three dynamo thresholds of different kind, (b) Dashed line merges at infinity, all crosspoints inside, (c) Eigenfunction forms at Rm^* (left) and Rm^{***} (right) and (d) (Colour online) Expanded self-crossing area. $\omega_c(Rm)$ is middle line between two branches of singular curve ($k_i = -0.0877$).

lasers where two light beams go in opposite directions. A notable difference concerns, however, the relevant lengths – lasers use to contain many wavelengths, the dynamo just a few.

The curve self-crossing in figure 8(b) occurs in a small k_i interval ($0.074 < -k_i < 0.0877$), where for experimental use is suitable only for a tiny part ($0.0847 < -k_i < 0.0877$). The crossing is at such a small angle that without magnification it is not visible. The approximate nature may raise doubts on the accuracy of the Rm^{***} determination from this intersection, on which relies the credibility of the whole project. Roughly speaking: the success of whole enterprise seems hidden in the third digit after the decimal point!

The source of this is in a sequence in which equation set (5a,b) is solved. Solving against Gauss rules is a bad practice of course. Nevertheless, while codes internal accuracy allow such and dependence on a single boundary parameter L appears smooth, the above explanation is meaningful. The problem is with solid velocity profiles only. Polynomial profiles expand figure 8(b) enough, and so there is no need for figure 8(d).

There are two better ways of solving:

(i) Rearranging variables between axis variables and curve parameters transfers figure 8 into figure 9. Intersection points (dots) in figure 9(b) are well defined

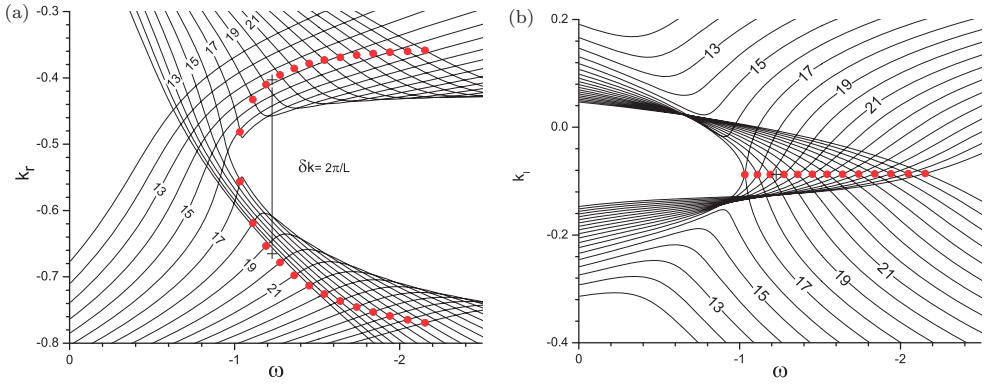

Figure 9. Figure 5 from Gailitis and Freibergs (1980b) adopted to our experiment. Curves are labeled by *Rm*.

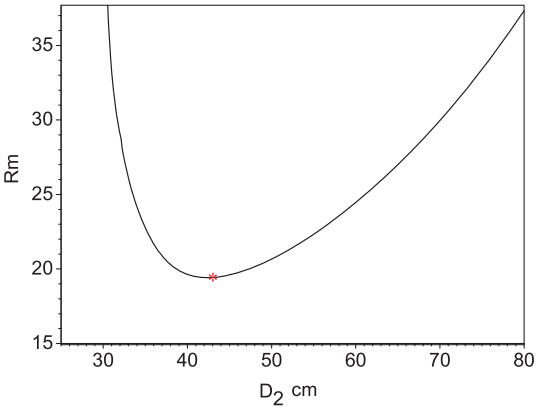

Figure 10. Optimization of reverse flow diameter D_2 at $D_1 = 25\,\text{cm}$ and $D_3 = 80\,\text{cm}$.

to find ω for each *Rm*. Vertical distance between corresponding dots in left plot gives $|k_1 - k_2| = 2\pi/L$. But for verbal discussion, figure 9 is less rich than figure 8.

(ii) It is numerically best to iterate (5a,b) by four-dimensional Newton-Raphson code with Gauss elimination rules included. We get all our numerical data this way. For any practical purpose all three ways are equally good.

Based on this model, the experiment was computed and numerically optimized for self-excitation at minimum *Rm*. Since the motor power consumption raises as Rm^3, the critical *Rm* has to be as small as possible for a successful experiment. The optimization, constrained by the given volume of sodium ($2m^3$), concerned four sizes: the total length, the outside diameter, and the two internal diameters. As an example, the critical *Rm* versus reverse-flow diameter is given in figure 10. The actual diameter is marked there with *. The rightmost point corresponds to the limit of a two-chamber version with the reverse-flow diameter equal to the external one. The unreachable *Rm* value indicates that without external sodium at rest the experiment would not be possible.

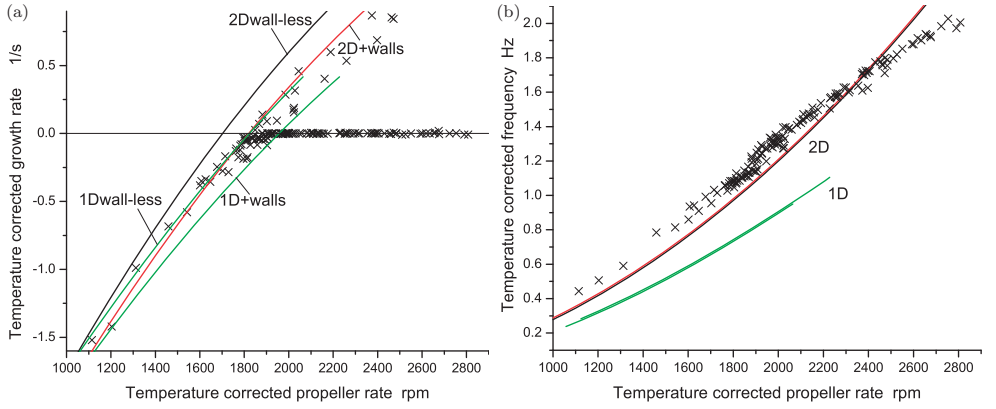

Figure 11. (Colour online). Observed field growth rate (a) and frequency (b) compared with prediction. 1D-present model, 2D-numerical integration on 2D grid. Internal wall resistance accounted/unaccounted.

Another optimization concerns the flow profile in the central cylinder. The propeller-generated velocity profile in the inner cylinder differs from the solid body motion. It is easy to take this into account by representing the measured velocity profiles by a polynomial approximation and the internal I-functions by the corresponding power series evaluated directly from equation (1). This creates no practical problem, because in most cases the internal I-function is computed from power series anyway. Testing different profiles numerically, the solid body profile was not found to be the best. Better profiles are characterized by an axial flow with a clear maximum at the center. In contrary, the azimuthal flow maximum has to be as far from center as possible. Without taking special measures the real situation in typical propeller wakes is opposite – usually the rotation concentrate close to the axis. To prevent this, two arrays of carefully designed vanes were installed both in front and behind the propeller. As a result, water tests in the actual dynamo module had shown acceptable profiles. After polynomial approximation they were included in our computer code to predict growth rates and frequencies (figure 11). The better flow shape happens to compensate for a somewhat too low rotation so that the generation starts close to solid body prediction.

The approximate character of the used model should always be kept in mind because the limited length experiment is treated as a very long one. Properly addressing the end problem, the internal field and current (field derivatives) should match the external solution which disappear at z infinity. Only for an infinitely long model (close to the absolute instability point Rm^{**}) is it sufficient to require $|k_1 - k_2|L = 2\pi$, as superposition $\exp(\mathrm{i}k_1 z) - \exp(\mathrm{i}k_2 z) = 2\mathrm{i}\sin[(k_1 - k_2)z/2]\exp[\mathrm{i}(k_1 - k_2)z/2]$ at the endpoints equals to zero and all its derivatives there tend to zero when k_1 tends to k_2 canceling external solution. Since the eigenfunction is composed of two solutions with different k values, the magnetic-field distribution depends on the radius. Any superposition of the two solutions reaches zero at a certain radius, but at other radii they differ from zero. Hence, at limited lengths, zeros at ends are not strictly ensured.

Despite all those uncertainties, the experiment was designed on the basis of the model sketched above and it actually works very close to what was expected.

5. Conclusions

This article touched upon two asymptotic approaches. Ponomarenko used the standard Bessel function asymptotic (i.e. asymptotic in radial direction). This appeared to give a sufficient proof of growing field existence, for which it was intended, but was not accurate enough to calculate the actual threshold of self-excitation. Contrarily, the asymptotic approach in axial direction, which seemed to be based on a potentially dubious assumptions, gave a satisfactory assessment of the generation threshold.

The main experimental result is that the experiment works and works very close to what was expected. Specifically our concerns are with the generation threshold, the spatial shape of the field and the main frequency. The saturated field is rather high, about 0.1T, i.e. about one order higher than in Karlsruhe. The record of the field time dependence is rather rich. Apart from the main frequency, we also see the third and fifth harmonics, two doublets from mixing main frequency with propeller and its wing rates and a long turbulent tail. Despite the presence of turbulence in frequency spectra it plays no role in a main generation process.

There remains much to be done. After enhancing cooling, we hope to run experiment at more stable temperature for exploring saturated field scaling properties, etc. By modifying velocity profiles there, it seems possible to reach even chaotic generation (Stefani *et al.* 2011).

Acknowledgments

The work was partly supported by European Commission under contract 028670.

References

Busse, F.H., A model of the geodynamo. *Geophys. R. Astron. Soc.* 1975, **42**, 437–459.

Gailitis, A., Self-excitation conditions for a laboratory model of a geomagnetic dynamo. *Magnetohydrodynamics* 1967, **3**, 45–54.

Gailitis, A., Magnetic field excitation by a system of submerged jets. *Magnetohydrodynamics* 1969, **5**, 20–24.

Gailitis, A., Self-excitation of a magnetic-field by a pair of annular vortices. *Magnetohydrodynamics* 1970, **6**, 14–17.

Gailitis, A., The Helical MHD Dynamo. In *Topological Fluid Mechanics: Proceedings IUTAM Symposium*, Cambridge, 1989, August 13–18, edited by H.K. Moffatt and A. Tsinober, pp. 147–156, 1989. (Cambridge University Press: Cambridge, UK).

Gailitis, A., Magnetic field generation by axisymmetric flows of conducting liquids in a spherical stationary conductor cavity. *Magnetohydrodynamics* 1993, **29**, 107–115.

Gailitis, A., Magnetic field generation by the axisymmetric conducting fluid flow in a spherical cavity of a stationary conductor, II. *Magnetohydrodynamics* 1995, **31**, 38–42.

Gailitis, A., Design of a liquid sodium MHD dynamo experiment. *Magnetohydrodynamics* 1996, **32**, 58–62.

Gailitis, A. and Freiberg, J., Theory of a helical MHD dynamo. *Magnetohydrodynamics* 1976, **12**, 127–129.

Gailitis, A. and Freiberg, J., Nonuniform model of a helical dynamo. *Magnetohydrodynamics* 1980a, **16**, 11–14.

Gailitis, A. and Freiberg, J., Nature of the instability of a turbulent dynamo. *Magnetohydrodynamics* 1980b, **16**, 116–121.

Gailitis, A., Karasev, B.G., Kirillov, I.R., Lielausis, O.A., Luzhanskii, S.M., Ogorodnikov, A.P. and Preslitskii, G.V., Experiment with a liquid-metal model of an MHD dynamo. *Magnetohydrodynamics* 1987, **23**, 349–352.

Gailitis, A., Karasev, B.G., Kirillov, I.R., Lielausis, O.A. and Ogorodnikov, A.P., The helical MHD dynamo. In *Liquid Metal Magnetohydrodynamics*, edited by J. Lielpeteris and R. Moreau, pp. 413–419, 1989. (Kluwer: Dordrecht).

Gailitis, A., Lielausis, O., Dement'ev, S., Platacis, E., Cifersons, A., Gerbeth, G., Gundrum, T., Stefani, F., Christen, M., Hänel, H. and Will, G., Detection of a flow induced magnetic-field eigenmode in the Riga dynamo facility. *Phys. Rev. Lett.* 2000, **84**, 4365–4368.

Gailitis, A., Lielausis, O., Platacis, E., Dement'ev, S., Cifersons, A., Gerbeth, G., Gundrum, T., Stefani, F., Christen, M. and Will, G., Magnetic field saturation in the Riga dynamo experiment. *Phys. Rev. Lett.* 2001a, **86**, 3024–3027.

Gailitis, A., Lielausis, O., Platacis, E., Dement'ev, S., Cifersons, A., Gerbeth, G., Gundrum, T., Stefani, F., Christen, M. and Will, G., Dynamo experiments at the Riga sodium facility. *Magnetohydrodynamics* 2002, **38**, 4–14.

Gailitis, A., Lielausis, O., Platacis, E., Gerbeth, G. and Stefani, F., On the results of Riga dynamo experiment. *Magnetohydrodynamics* 2001b, **37**, 3–12.

Gailitis, A., Lielausis, O., Platacis, E., Gerbeth, G. and Stefani, F., Riga Dynamo Experiment. In *Dynamo and Dynamics: A Mathematical Challenge*, NATO Science Series II: Mathematics, Physics and Chemistry, edited by P. Chossat, D. Armbruster and I. Oprea, Vol. 26, pp. 9–16, 2001c. (Kluwer: Dordrecht).

Gailitis, A., Lielausis, O., Platacis, E., Gerbeth, G. and Stefani, F., Riga dynamo experiment and its theoretical background. *Phys. Plasmas* 2004, **11**, 2838–2843.

Landau, L.D. and Lifshitz, E.M., *Mechanics of Continuous Media*, 1954. (Moskow: Gostechizdat) (in Russian).

Müller, U. and Stieglitz, R., Can the Earth's magnetic field be simulated in laboratory? *Naturwissenschaften* 2000, **87**, 381–390.

Pitaevskii, L.P. and Lifshitz, E.M., *Physical Kinetics*, 1st ed., Vol. 10, 1981. (Oxford: Pergamon Press) (ISBN 978-0-750-62635-4).

Ponomarenko, Yu.B., On the Theory of Hydromagnetic Dynamo. *J. Appl. Mech. Tech. Phys.* 1973, **14**, 775–779.

Roberts, G.O., Dynamo action of fluid motions with two-dimensional periodicity. *Philos. Trans. R. Soc. London* 1972, **A 271**, 411–454.

Schubauer, G.B. and Skramstad, H.K., Laminar-boundary-layer oscillations and transitions on a flat plate. NACA Report. 909, 1947.

Steenbeck, M., Kirko, I.M., Gailitis, A., Klavina, A.P., Krause, F., Laumanis, I.J. and Lielausis, O.A., Der experimentelle Nachweis einer elektromotorischen Kraft längs eines äußeren Magnetfeldes, induziert durch eine Strömung flüsigen Metalls (alpha-Effekt). *Monatsberichte der DAW* 1967, **9**, 714–719.

Steenbeck, M., Kirko, I.M., Gailitis, A., Klavina, A.P., Krause, F., Laumanis, I.J. and Lielausis, O.A., An experimental verification of alpha effect. *Dokladi Ac. Sci USSR* 1968, **180**, 326–329.

Steenbeck, M., Krause, F. and Rädler, K.-H., A calculation of the mean electromotive force in an electrically conducting fluid in turbulent motion, under the influence of Coriolis forces. *Z. Naturforsch.* 1966, **21a**, 369–376.

Stefani, F., Gailitis, A. and Gerbeth, G., Energy oscillations and a possible route to chaos in a modified Riga dynamo. *Astron. Nachr.* 2011, **332**, 4–10.

Stefani, F., Gerbeth, G. and Gailitis, A., Velocity profile optimization for the Riga dynamo experiment. In *Transfer Phenomena in Magnetohydrodynamic and Electroconducting Flows*, edited by A. Alemany and Ph. Marty, pp. 31–44, 1999. (Kluwer: Dordrecht).

Stieglitz, R. and Müller, U., Experimental demonstration of a homogeneous two-scale dynamo. *Phys. Fluids* 2001, **13**, 561–564.

Stieglitz, R. and Müller, U., Experimental demonstration of a homogeneous two-scale dynamo. *Magnetohydrodynamics* 2002, **38**, 27–33.